Atmos. Meas. Tech., 10, 2077–2091, 2017
https://doi.org/10.5194/amt-10-2077-2017

Atmospheric Measurement Techniques
Open Access

Characterization of interferences to in situ observations of $\delta^{13}CH_4$ and C_2H_6 when using a cavity ring-down spectrometer at industrial sites

Sabina Assan, Alexia Baudic, Ali Guemri, Philippe Ciais, Valerie Gros, and Felix R. Vogel

Laboratoire des Sciences du Climat et de l'Environnement, Chaire BridGES, UMR CNRS-CEA-UVSQ,
Gif-sur-Yvette, Ile-de-France, 91191, France

Correspondence to: Sabina Assan (sabina.assan@lsce.ipsl.fr)

Received: 2 August 2016 – Discussion started: 19 December 2016
Revised: 8 March 2017 – Accepted: 15 March 2017 – Published: 7 June 2017

Abstract. Due to increased demand for an understanding of CH_4 emissions from industrial sites, the subject of cross sensitivities caused by absorption from multiple gases on $\delta^{13}CH_4$ and C_2H_6 measured in the near-infrared spectral domain using CRDS has become increasingly important. Extensive laboratory tests are presented here, which characterize these cross sensitivities and propose corrections for the biases they induce. We found methane isotopic measurements to be subject to interference from elevated C_2H_6 concentrations resulting in heavier $\delta^{13}CH_4$ by $+23.5$ ‰ per ppm C_2H_6 / ppm CH_4. Measured C_2H_6 is subject to absorption interference from a number of other trace gases, predominantly H_2O (with an average linear sensitivity of 0.9 ppm C_2H_6 per % H_2O in ambient conditions). Yet, this sensitivity was found to be discontinuous with a strong hysteresis effect and we suggest removing H_2O from gas samples prior to analysis. The C_2H_6 calibration factor was calculated using a GC and measured as 0.5 (confirmed up to 5 ppm C_2H_6). Field tests at a natural gas compressor station demonstrated that the presence of C_2H_6 in gas emissions at an average level of 0.3 ppm shifted the isotopic signature by 2.5 ‰, whilst after calibration we find that the average $C_2H_6:CH_4$ ratio shifts by $+0.06$. These results indicate that, when using such a CRDS instrument in conditions of elevated C_2H_6 for CH_4 source determination, it is imperative to account for the biases discussed within this study.

1 Introduction

With increasing efforts to mitigate anthropogenic greenhouse gas emissions, opportunities to reduce leaks from fossil fuel derived methane (ffCH_4) are of particular importance as they currently account for approximately 30 % of all anthropogenic methane emissions (Kirschke et al., 2013). At present, technically feasible mitigation methods hold the potential to half future global anthropogenic CH_4 emissions by 2030. Of this mitigation potential more than 60 % can be realized in the fossil fuel industry (Hoglund-Isaksson, 2012). However, for effective implementation, sources, locations and magnitudes of emissions must be well known.

The global increase in the production and utilization of natural gas, of which methane is the primary component, has brought to light questions in regards to its associated fugitive emissions, i.e. leaks. Recent estimates of CH_4 leaks vary widely (1–10 % of global production; Allen, 2014) and US inventories of natural gas CH_4 emissions have uncertainties of up to 30 % (US EPA, 2016). In addressing this issue, the ability to distinguish between biogenic and different anthropogenic sources is of vital importance. For this reason methane isotopes ($\delta^{13}CH_4$) are commonly used to better understand global and local emissions, as demonstrated in a number of studies (Lamb et al., 1995; Lowry et al., 2001; Hiller et al., 2014). The discrimination of sources with relatively close isotopic composition such as oil-associated gas and natural gas, which can have isotopic signatures separated by only ∼4 ‰ (Stevens and Engelkemeir, 1988), requires precise and reliable $\delta^{13}CH_4$ measurements.

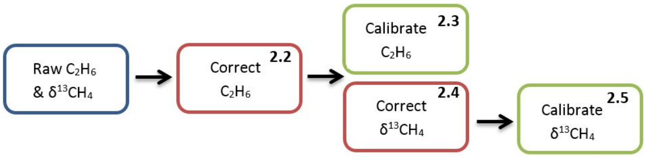

Figure 1. Flow chart illustrating the steps involved to calibrate C_2H_6 and $\delta^{13}CH_4$. The number in the top right-hand corner corresponds to the subsection in which the methods of each step are explained in detail.

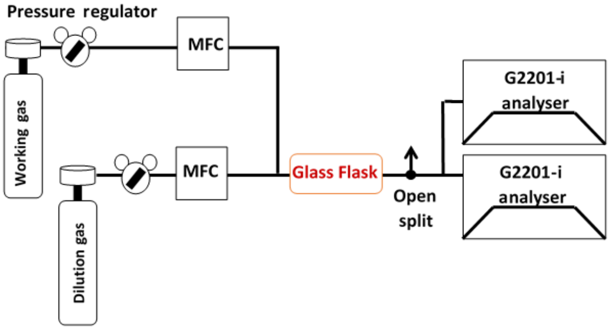

Figure 2. General set-up. The dilution and working gas are connected via two MFCs to two CRDS instruments in parallel. In red is the placement of an optional glass flask used for the C_2H_6 calibration only. The flow is greater than that of the instruments' inlets. Therefore an open split is included to vent additional gas and retain ambient pressure at the inlets.

Ethane (C_2H_6) is a secondary component in natural gas and can be used as a marker to distinguish between different CH_4 sources. Use of the C_2H_6 : CH_4 ratio provides a robust identifier for the gas of interest. Recent findings in the US found coal bed C_2H_6 : CH_4 ratios ranging between 0 and 0.045, while dry and wet gas sources displayed differing ratios of < 0.06 and > 0.06 respectively (Yacovitch et al., 2014; Roscioli et al., 2015).

Laser spectrometers, especially those based on cavity ring-down spectroscopy (CRDS), are now a common deployment for site-scale CH_4 measurement campaigns (Yvon-Lewis et al., 2011; Phillips et al., 2013; Subramanian et al., 2015). However, with the advent of such novel technologies, there is a risk of unknown interference from laser absorption which can create biases in measurements. Some examples of this are discussed in Rella et al. (2015) and many others (e.g. Malowany et al., 2015; Vogel et al., 2013; Nara et al., 2012). Using a CRDS instrument we show that the presence of C_2H_6 causes significant interference to the measured $^{13}CH_4$ spectral lines, thus resulting in shifted reported $\delta^{13}CH_4$ values. We propose a method to correct these interferences and test it on measurements of natural gas samples performed at an industrial natural gas site.

The CRDS instruments used throughout this study are Picarro G2201-i analysers (Picarro INC, Santa Clara, USA) which measure gases including CH_4, CO_2, H_2O, and, although not intended for use by standard users, C_2H_6. This model measures in three spectral ranges: lasers measuring spectral lines at roughly 6057, 6251 and 6029 cm^{-1} are used to quantify mole fractions of $^{12}CH_4$, $^{12}CO_2$ and $^{13}CO_2$, and $^{13}CH_4$, H_2O and C_2H_6 respectively. The spectrograms are fit with two non-linear models in order to determine concentrations; the primary fit excludes the model function of C_2H_6 while the second includes this function, thus adding the ability to measure C_2H_6 (Rella et al., 2015). Such a method for measuring C_2H_6 concentrations is crude, thus the uncalibrated C_2H_6 concentration data are stored in private archived files which until now have been used primarily for the detection of sample contamination. The measurements of $\delta^{13}CH_4$ and $\delta^{13}CO_2$ are calculated using the ratios of the concentrations of $^{12}CH_4$, $^{13}CH_4$, $^{12}CO_2$ and $^{13}CO_2$ respectively.

An experimental procedure is presented here which corrects the interference caused by C_2H_6 on the retrieval of $\delta^{13}CH_4$ using such a CRDS instrument for application to in situ or continuous measurements of $\delta^{13}CH_4$ strongly contaminated by C_2H_6, i.e. in the vicinity of ffCH_4 sources. The step-by-step procedure of the experimental methods developed to quantify the cross sensitivities and the proposed calibration for $\delta^{13}CH_4$ and C_2H_6 are depicted in Fig. 1 and presented in detail in Sect. 2. Section 3 encompasses a discussion of the results, including an analysis of the instrumental responses for two spectrometers with an evaluation of the stability and repeatability of the suggested corrections. Finally, field measurements were performed at a natural gas compressor station where the aim was to identify emissions between two natural gas pipelines. In Sect. 5 the importance of the corrections for field measurements is demonstrated by applying our methods to data retrieved during this period while also revealing the instruments' potential to measure C_2H_6.

2 Methods

The purpose of laboratory tests was to characterize the instruments' response to concentration changes in gases found at fossil fuel sites (e.g. gas extraction or compressor stations), specifically, the cross sensitivities of CO_2, CH_4 and H_2O on C_2H_6 and of C_2H_6 on $\delta^{13}CH_4$. Presumably there are additional gases with the potential for interference; this study focuses on those reported to have a significant effect on C_2H_6 and $\delta^{13}CH_4$ measurements by Rella et al. (2015). We also define and describe a new procedure to calibrate both C_2H_6 and $\delta^{13}CH_4$.

In the following chapter the general set-up used for the majority of experiments is described, after which we enter a more detailed description of the processes involved in each step.

Table 1. Description of the gas mixtures used to determine the cross-sensitivities of the interference of CH_4, H_2O and CO_2 on C_2H_6 and the interference of C_2H_6 on $\delta^{13}CH_4$. The respective ranges spanned during laboratory tests, and the typical range at a natural gas site are noted on the right-hand side.

		Method	Dilution gas	Working gas	Lab concentration Range	Typical range at NG site
H_2O interference on C_2H_6	< 0.16 % (dry) ≥ 0.16 % (wet)	Magnesium perchlorate Dilution series & humidifier	N/A	Ambient air Zero air	0–0.5 % H_2O 0.25–2.5 % H_2O	0–2 % H_2O
CO_2 interference on C_2H_6	< 0.16 % (dry) ≥ 0.16% (wet)	Dilution series Dilution series & humidifier	Zero air 1.7 ppm CH_4,	2000 ppm CO_2, < 1 ppb C_2H_6 and 50 ppb CO in natural air	0–1500 ppm CO_2 0–1500 ppm CO_2, 0.5–1.5 % H_2O	400–1000 ppm CO_2
CH_4 interference on C_2H_6	< 0.16 % (dry) ≥ 0.16 % (wet)	Dilution series & ascarite Dilution series, ascarite & humidifier	Zero air 310 ppb N_2O, < 1 ppb C_2H_6	6 ppm CH_4, 360 ppm CO_2, and 50 ppb CO in natural air	0–6 ppm CH_4 0–6 ppm CH4, 1 %H_2O	2–20 ppm CH_4
C_2H_6 interference on $\delta^{13}CH_4$	Dilution series (CRDS)	Natural air matrix (< 1 ppb C_2H_6)	C_2H_6 standard of 52 ppm in nitrogen	0–1.5 ppm C_2H_6/ ppm CH_4	0–0.3 ppm C_2H_6/ ppm CH_4	
C_2H_6 calibration	Dilution series (CRDS & GC)	Natural air matrix (< 1 ppb C_2H_6)	C_2H_6 standard of 52 ppm in nitrogen	0–5 ppm C_2H_6	0.3–3 ppm C_2H_6	

2.1 Experimental set-up

2.1.1 Method

Each cross sensitivity is measured by creating a gas dilution series designed to control the concentrations of the gas responsible for the interference in steps while keeping concentrations of the other gas components constant (in particular the component subject to interference). The instrument response was evaluated for a large range of concentrations and different combinations of gas components. An example of such a measurement time series can be seen in Fig. S1 in the Supplement. The experimental set-up used includes two CRDS instruments (Picarro G2201-i) running in parallel in a laboratory at ambient conditions (25 °C, 100 m above sea level; a.s.l). The instruments were used in iCO_2-iCH_4 auto switching mode, of which we consider only the "high precision" mode of $\delta^{13}CH_4$ throughout the study. For the dilution series, a working gas is diluted in steps using a set-up of two mass flow controllers (MFC; El-flow, Bronkhorst, Ruurlu, the Netherlands), as shown in Fig. 2. A T-junction splits the gas flow to both instruments; the total flow is greater than the flow drawn into the instruments. Hence to maintain an inlet pressure close to ambient, the set-up includes an open split to vent additional gas. In order to assess variability and error, each experiment is repeated a minimum of three times consecutively. To detect instrumental drift between experiments, a target gas is measured before commencing each dilution sequence. An overview of each targeted cross interference, with information on the gases used and ranges spanned in laboratory tests, can be found in Table 1.

2.1.2 Gases

Throughout the experiments, four categories of gas were used: a zero air gas with measured residual concentrations of < 1 ppm CO_2, < 30 ppb CH_4 , ≈ 170 ppb CO, < 1 ppb C_2H_6 (Deuste-Steininger,Walldorf, Germany), working gases with variable concentrations of CO_2 and CH_4 in a natural air matrix (Deuste-Steininger,Walldorf, Germany), a C_2H_6 standard of 52 ppm in nitrogen (National Physics Laboratory (NPL), Teddington, United Kingdom), and dried ambient air in 40L aluminium cylinders filled using an oil-free RIX compressor (RIX industries, Benicia, USA). Details of the gas mixture used in each dilution series depends on the response targeted within the experiment. This information can be found in Table 1 and is also discussed in further detail throughout this chapter.

2.2 Determination of C_2H_6 corrections from H_2O, CH_4 and CO_2 interference

The value of C_2H_6 based on the standard CRDS data processing package (hereafter, the raw value) is biased by cross-sensitivities with H_2O, CO_2 and CH_4. Experiments were conducted at different constant C_2H_6 concentrations so that any shifts in the raw C_2H_6 are due to the cross sensitivity to other components in the measured samples. To alter the water vapour content of a sample, the experimental set-up described in Fig. 2 was modified by incorporating a humidifier. The humidifier consists of a liquid flow controller (Liquiflow, Bronkhorst, Ruurlu, the Netherlands) and a mass flow controller (El-flow, Bronkhorst, Ruurlu, the Netherlands) fed into a controlled evaporator mixer (CME) (Bronkhorst, Ruurlu, the Netherlands). The tube departing the CME contains a gas flow of 2 L min^{-1} and is heated to 40 °C to prevent any condensation. A short description and diagram of the humidifying bench can found in Laurent et al. (2015).

The H_2O interference on C_2H_6 was measured by using the humidifier to vary the H_2O content of zero air gas in the range of 0.25–2.5 % H_2O, representing the range of real world conditions. The humidifier set-up cannot reliably reach humidity below 0.2 % H_2O, a range frequently reached when measuring gas cylinders or dried air. This low range was attained using a H_2O scrubber (Magnesium Perchlorate, Fisher Scientific, Loughborough, UK) connected to the CRDS instrument inlet while measuring ambient air. As the efficiency of the scrubber decreases over time, a slow increase of H_2O spanning low concentrations in the range of 0–0.5 % can be observed.

The CH_4 interference on C_2H_6 was measured by creating a dilution series of variable CH_4 content using zero air and a working gas of 6 ppm CH_4, 360 ppm CO_2, 310 ppb N_2O and 50 ppb CO in natural air. Methane concentrations ranged from 0 to 6 ppm. To keep other causes of interference at a minimum, the gas mixture passed through two scrubbers: the first a CO_2 scrubber (Ascarite(ii), Acros Organics, USA) and the second a H_2O scrubber (Magnesium Perchlorate, Fisher Scientific, Loughborough, UK). As an independent check on the linearity of the response functions, each dilution sequence was repeated at two humidities (0 % H_2O and 1 % H_2O) and four C_2H_6 concentrations (between 0 and 1.5 ppm).

The CO_2 interference on C_2H_6 was measured with a dilution series ranging 0–1500 ppm CO_2 created by mixing zero air and a working gas of 2000 ppm CO_2, 1.7 ppm CH_4 and 50 ppb CO in natural air. Any interference due to CH_4 was accounted for during data processing. This test was repeated at four water vapour levels (0, 0.5, 1 and 1.5 %) and five C_2H_6 concentrations (between 0 and 2.5 ppm).

2.3 C_2H_6 calibration set-up

In order to correctly use the C_2H_6 data from CRDS instruments, the data must be calibrated to an internationally recognized scale. To achieve this, the set-up described in Sect. 2.1 was modified to include the filling of removable samples (1 L glass flasks), the concentrations of which could be independently verified, as shown in Fig. 2. A gas mixture using the C_2H_6 standard and an ambient air cylinder was created via two MFCs before passing through the flask on its way to the instruments' inlets. Each step in the dilution series requires an individual flask, which was flushed for 20 min and then analysed for 10 min with an average precision of 0.02 ppm C_2H_6 on the CRDS instrument. The flask is subsequently sealed and removed for analysis on a gas chromatograph (GC) (Chrompack Varian 3400, Varian Inc, USA) which uses National Physics Laboratory (NPL) standards and has an uncertainty better than 5 %. The system is described in more detail in Bonsang and Kanakidou (2001).

In total 17 flasks were filled with gas mixtures spanning from 0 to 5 ppm C_2H_6, covering the range expected near a leak of ffCH_4 (Gilman et al., 2013; Jackson et al., 2014). In order to calibrate the linearity of the response at very high concentrations which may be expected from pure natural gas samples, we conducted a measurement at 100 % of the C_2H_6 standard (52 ppm ± 1 ppm).

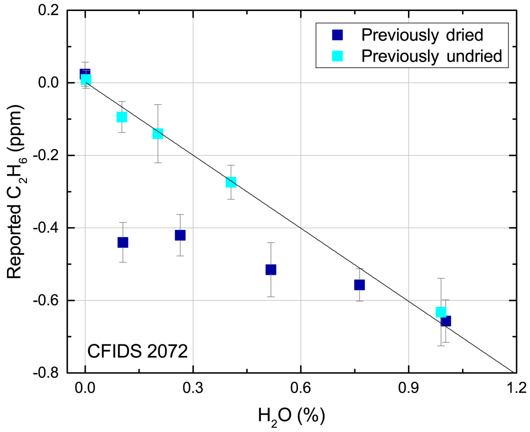

Figure 3. An example of the results from a H_2O interference experiment spanning the range 0–1 % H_2O. The reported C_2H_6 is altered due to the addition of water vapour when measuring zero air (< 1 ppb C_2H_6). Dark and light blue markers signify the response when dried and undried ambient air have been measured overnight by the instrument prior to the experiment respectively. Error bars signify the standard deviation of each measurement.

2.4 Determining the correction for $\delta^{13}CH_4$

Measured $\delta^{13}CH_4$ is altered in the presence of C_2H_6. To understand the magnitude of this effect, experiments were conducted using the method described in Sect. 2.1. The dilution series uses the C_2H_6 standard and a cylinder filled with ambient air, i.e. with a negligible C_2H_6 mixing ratio (< 1 ppb), to create concentration values spanning from 0 to 4 ppm C_2H_6. As there is only one source of CH_4 in the experiment, the addition of C_2H_6 should not affect the value of $\delta^{13}CH_4$; hence any change seen is an apparent shift of $\delta^{13}CH_4$ due to C_2H_6 interference. This concentration range was chosen as it encompasses a $C_2H_6 : CH_4$ ratio of 0 to 1, well within the likely range to be measured from fossil fuel sources (Yacovitch et al., 2014).

2.5 Calibration of $\delta^{13}CH_4$

The reported $\delta^{13}CH_4$ was calibrated to Royal Holloway University of London (RHUL) scale using four calibration gases spanning −25 to −65 ‰ that were created by different dilutions of pure CH_4 and CO_2 with ambient air. The aliquots were measured multiple times by isotope ratio mass spectrometry (IRMS) at RHUL. The precision for $\delta^{13}CH_4$, obtainable with this IRMS, is reported as 0.05 ‰ – detailed information on the measurement system can be found in Fisher et al. (2006). The calibration factor is determined from a linear regression and calibrations were performed once a day for 3 consecutive days before and after the laboratory experiments. A target gas was measured regularly to track any drift in $\delta^{13}CH_4$ as an independent check on the calibration quality.

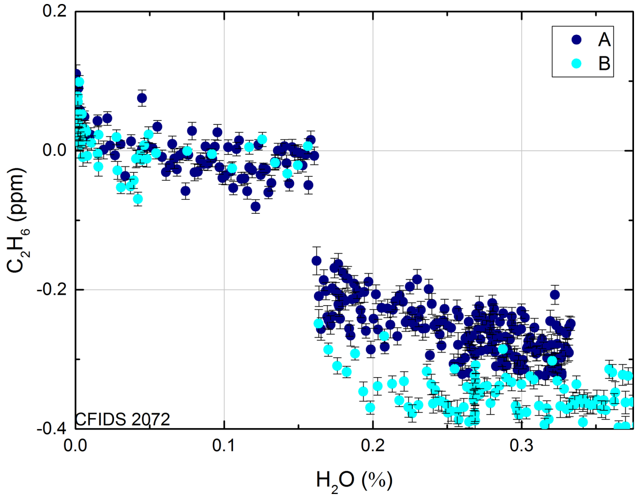

Figure 4. The discontinuity seen for instrument CFIDS 2072 for two repetitions denoted by different colours. After the discontinuity at 0.16 % the subsequent slope clearly differs between the two repetitions. Both instruments display a discontinuity at 0.16 % H_2O. Each point represents a 1 min average, the error bars represent the standard deviation of the raw data.

3 Results and discussion

This study focuses on determining a reliable correction and calibration scheme for a Picarro G2201-i when measuring methane sources with C_2H_6 interference. Findings from the experiments described in Sect. 2 are discussed in detail here.

In order to calibrate $\delta^{13}CH_4$ and C_2H_6 values, there are a series of corrections that must take place beforehand (see Fig. 1). The initial correction to be applied is on C_2H_6 due to interference from CH_4, CO_2 and H_2O. Particular emphasis is placed on this correction due to the discovery of significant non-linear behaviour in the presence of H_2O, CH_4 and CO_2 in the sample gas. Once the C_2H_6 has been corrected, the calibration of C_2H_6 using independent GC measurements, the C_2H_6 interference correction on $\delta^{13}CH_4$ and finally the calibration of $\delta^{13}CH_4$ can be effected.

For our results to be applicable to future studies we examine the inter-instrument variability and stability over time, compare our results to current literature and discuss the uncertainties attributed to our results. Throughout this study we refer to raw, uncorrected C_2H_6 and $\delta^{13}CH_4$ concentrations as "reported" to highlight that they may be influenced by interferences and are uncorrected. Within this section negative C_2H_6 concentrations are often mentioned. We note that this is the "reported" C_2H_6 concentration by the instrument. Unless otherwise stated, the standard deviation reported is calculated from 1 min averages and depicted as error bars within figures.

3.1 Correcting reported C_2H_6

3.1.1 H_2O interference on C_2H_6

H_2O content was found to be the dominating source of interference to reported C_2H_6; its presence decreases the reported concentration of C_2H_6 with increasing H_2O concentration. Furthermore, the response function exhibits a hysteresis effect, which, although small, can be considerable when changing from dry to undried air samples (e.g. between dry calibration gas and undried ambient air). There are two distinct instrumental responses, depending on whether dried or undried ambient air are being measured during the night preceding the experiment, which are depicted in Figure 3 by dark and light blue markers respectively. When the CRDS instrument measures dry air prior to the experiment, a discontinuity is observed at 0.16 % H_2O. Figure 4 shows this effect in more detail; prior to 0.16 % H_2O the response function exhibits a stable linear response. The correction within this low range was found to be the same for both instruments, 0.44 ± 0.03 ppm C_2H_6 / % H_2O. After passing the 0.16 % H_2O threshold, the response exhibits a discontinuity with a magnitude and subsequent slope that are also dependent on the air moisture beforehand. This is seen in Fig. 4 whereby the discontinuity of two repetitions (A and B depicted by dark and light blue markers respectively) differs in magnitude by 0.1 ppm reported C_2H_6. The discontinuity occurs when the instrument passes the 0.16 % H_2O threshold, both when moving from dry to wet air and vice versa (see Fig. S2). If measuring undried air before the experiment, the interference due to H_2O can be described well by a linear response (light blue markers in Fig. 3) and potentially causes large biases from the true C_2H_6. For example, if measuring at 1 % H_2O, both instruments display a change in reported C_2H_6 of approximately -0.9 ppm. The response function calculated for instruments CFIDS 2072 and 2067 differed, showing -0.72 ± 0.03 ppm C_2H_6 / % H_2O and -1.00 ± 0.01 ppm C_2H_6 / % H_2O with R^2 values of 0.98 and 0.99 respectively. The hysteresis effect is evident when measuring with undried air; the slope was seen to shift after each repetition, in total by 0.1 ppm C_2H_6 / % H_2O.

3.1.2 CO_2 interference on C_2H_6

For both instruments an increase in the CO_2 concentration results in lower reported values of C_2H_6, and it is furthermore apparent that the magnitude of this interference is dependent on air humidity. For a dry sample gas ($H_2O < 0.16$ % – demonstrated in the left-hand column of Fig. 5), the interference for both instruments is found to be highly stable and well characterized by a linear slope of $1 \times 10^{-4} \pm 1 \times 10^{-5}$ ppm C_2H_6 / ppmCO_2 with a R^2 value of 0.9. There was no measurable difference in slope at any of the C_2H_6 concentrations tested (see Fig. S3). In contrast, for water vapour levels ≥ 0.5 % H_2O (see right-

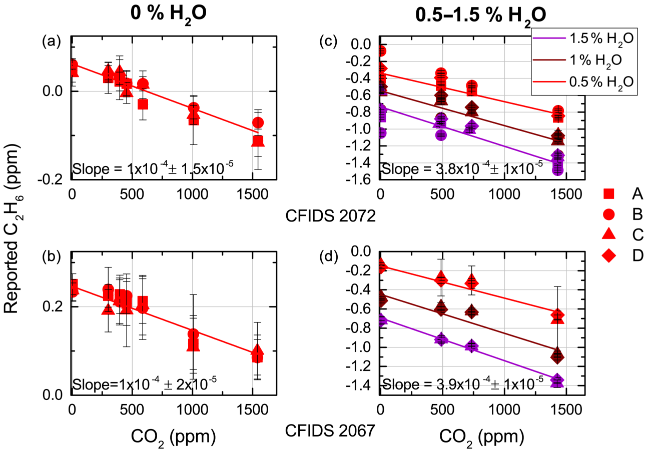

Figure 5. Relationship between reported C_2H_6 and concentration changes of CO_2 for instruments CFIDS 2072 and 2067 at varying values of H_2O, at 0 ppm C_2H_6 (within our instrumental precision). For each plot the bottom axis indicates the concentration of the targeted gas (CO_2). Plots **(a)** and **(b)** are at 0 % H_2O, **(c)** and **(d)** are experiments at varying humidities, distinguishable by colour. The legend denotes repetitions of the experiment. The error bars in each plot denote the standard deviation of each measurement. The R^2 values for the experiments at 0 % H_2O are 0.9 and 0.8 for all other H_2O experiments for both instruments.

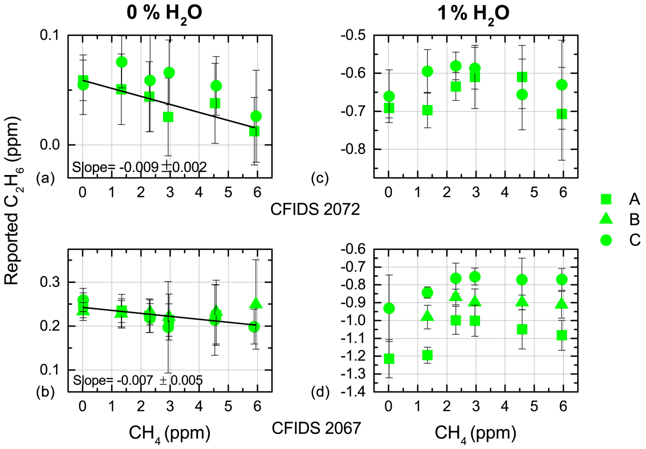

Figure 6. Relationship between reported C_2H_6 and concentration changes of CH_4 for both instruments at 0 ppm C_2H_6 (within our instrumental precision). For each plot, the bottom axis indicates the increase in concentration of the targeted gas. The vertical bars in each plot denote the standard deviation of each point. The legend denotes repetitions of the experiment. Plots **(a)** and **(b)** are at 0 % H_2O. The R^2 values are 0.4 and 0.6 for instruments CFIDS 2072 and 2067. Plots **(c)** and **(d)** show the response at 1 % H_2O. These two plots have a R^2 value of 0.2.

hand column of Fig. 5), measurements exhibit a higher scatter between repetitions. This is mainly attributed to a drifting intercept; however the experiments also show a smaller R^2 of 0.8. We calculate a characteristic linear slope of $3.8 \times 10^{-4} \pm 1 \times 10^{-5}$ ppm C_2H_6 / ppm CO_2 and $3.9 \times 10^{-4} \pm 1 \times 10^{-5}$ for ≥ 0.5 % water vapour for instruments CFIDS 2072 and 2069 respectively. Therefore, when measuring undried ambient air, the presence of CO_2 at a level near 400 ppm will induce a shift in the reported C_2H_6 of approximately -0.15 ppm C_2H_6, whereas if the air is dried the reported shift is much smaller, at approximately -0.04 ppm C_2H_6.

3.1.3 CH_4 interference on C_2H_6

The CH_4 effect on C_2H_6, as shown in Fig. 6, is less prominent by at least an order of magnitude than both the H_2O and CO_2 interferences. At dried ambient CH_4 concentrations a typical change in reported C_2H_6 of approximately -0.008 ppm is observed within both instruments. Dried air experiments show a high scatter of points between repetitions, and R^2 values of 0.4 and 0.6 for instruments CFIDS 2072 and 2067 respectively are calculated. Despite its large uncertainty, the data suggest that both instruments display a similar response with a statistically significant slope within the range of C_2H_6 concentrations tested (see Fig. S3). In light of this we use a weighted mean to calculate a linear response of $9 \times 10^{-3} \pm 2 \times 10^{-3}$ ppm C_2H_6 / ppm CH_4 for dry air measurements for CFIDS 2067, and $7 \times 10^{-3} \pm 5 \times 10^{-3}$ ppm C_2H_6 / ppm CH_4 for CFIDS 2072. The results obtained at 1 % H_2O show little correlation (as shown in the right-hand column of Fig. 6), with both instruments displaying a R^2 value of 0.2. An ANOVA test suggests the slopes are not significantly different from zero; thus we omit a CH_4 correction for this case.

3.1.4 Combining the CO_2, CH_4 and H_2O correction on C_2H_6

To fully take into account all (known) C_2H_6 cross-sensitivities, the corrections to reported C_2H_6 need to be combined. Due to the non-linearity of the discontinuity in reported C_2H_6 at 0.16 % H_2O and its subsequent slope we choose to report correction coefficients for the two found linear regimes, i.e. for continuous measurements with sample humidities below 0.16 % and sample humidities above 0.16 %. Within each range the proposed correction formula is given as follows:

$$(C_2H_6)_{\mathrm{CORRECTED}} = (C_2H_6)_{\mathrm{RAW}} + A^*(H_2O) + B^*(CH_4) + C^*(CO_2). \quad (1)$$

If the humidity is limited to less than 0.16 % before and during measurements, $A = 0.44 \pm 0.03$ ppm C_2H_6 / % H_2O, $B = 8 \times 10^{-3} \pm 2 \times 10^{-3}$ ppm C_2H_6 / ppm CH_4, $C = 1 \times 10^{-4} \pm 1 \times 10^{-5}$ ppm C_2H_6 / ppm CO_2. Both instruments demonstrated good agreement for all the correction factors calculated at < 0.16 % H_2O.

Corrections for measurements undertaken at concentrations higher than or equal to 0.16 % H_2O are $A =$

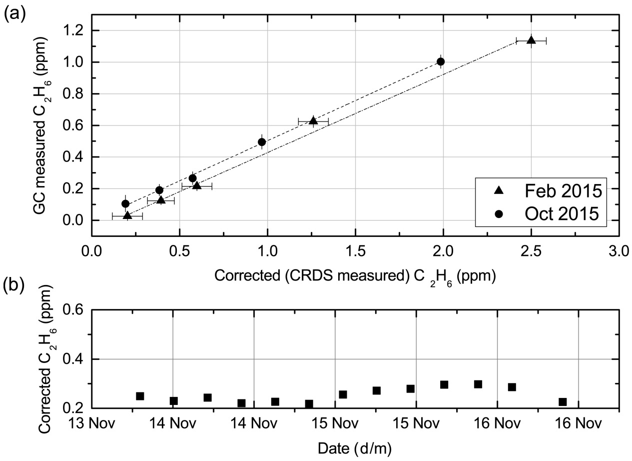

Figure 7. (a) Ethane calibration calculated from measurements of flask samples by both the GC and CRDS. The *x*-axis is the corrected C_2H_6 ($C_2H_{6\,\mathrm{COR}}$) using the corrections described previously. The *y*-axis is the C_2H_6 as measured by a manual GC. The error bars indicate the standard deviation of each flask measurement, for certain flasks error bars are smaller than their respective markers. **(b)** 30 min target measurements over a period of 4 days, from 13 to 16 November 2015. The standard error of each target is smaller than the plotted marker. The baseline C_2H_6 is seen to drift with time.

0.7 ± 0.03 ppm C_2H_6 / % H_2O, $B =$ 0 ppm C_2H_6 / ppm CH_4, $C =$ $3.8 \times 10^{-4} \pm 2 \times 10^{-5}$ ppm C_2H_6 / ppm CO_2 for CFIDS 2072 and $A =$ 1 ± 0.01 ppm C_2H_6 / % H_2O, $B = 0$ ppm C_2H_6 / ppm CH_4, $C = 3.9 \times 10^{-4} \pm 2 \times 10^{-5}$ ppm C_2H_6 / ppm CO_2 for CFIDS 2067.

3.2 C_2H_6 calibration

To make use of the corrected C_2H_6 it should be calibrated to match an internationally recognized scale. This is achieved by measuring whole-air samples by CRDS and independently on a calibrated gas chromatograph, as discussed within Sect. 2. The calibration factor is determined by comparing the corrected C_2H_6 resulting from CRDS and C_2H_6 as confirmed by the GC and plotted in Fig. 7a. The relationship was found to be linear throughout the range of 0–5 ppm C_2H_6 with a slope of 0.505 ± 0.007 and 0.52 ± 0.01 for instruments CFIDS 2072 and 2067 respectively. The results are reported in Table 2 from which we can see the intercept of the calibration for instrument CFIDS 2072 shifts between the experiment in February and that in October, while the slope remains constant throughout the measured time period. The change in the intercept is attributed to a C_2H_6 baseline drift which we have monitored over time using regular target gas measurements; an example is given in Fig. 7b. To account for this drift and any elevated baselines (such as that of CFIDS 2067 – see Table 2), a regular measurement of a working gas is necessary, from which the instrument offset can be calculated. For the full calibration, we thus suggest using Eq. (2), where D is the calibration factor (slope) for the instrument, i.e. for CFIDS 2072 $D = 0.505 \pm 0.007$ and Δ (WGS) the baseline drift determined using the working gas.

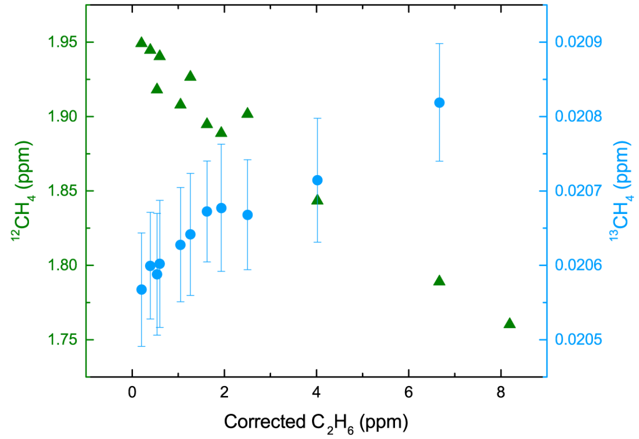

Figure 8. During a dilution sequence of ambient gas with C_2H_6, the CH_4 concentration decreases from its nominal concentration 1948.7 ppb ± 0.32 ,ppb as the contribution from C_2H_6 is increased. Thus both $^{12}CH_4$ and $^{13}CH_4$ undergo a similar decrease as the gas is diluted. However, what is observed is an increase in the reported value of $^{13}CH_4$, suggesting C_2H_6 interference. The $^{12}CH_4$ axis is plotted to the left in light green, whereas the $^{13}CH_4$ axis is plotted to the right in dark green at a different scale. Error bars represent the standard deviation, the $^{12}CH_4$ markers are larger than their associated error bars.

$$(C_2H_6)_{\mathrm{calibrated}} = D^*((C_2H_6)_{\mathrm{corrected}} - \Delta(\mathrm{WGS})) \qquad (2)$$

3.3 $\delta^{13}CH_4$ correction

By measuring the shift of the reported $\delta^{13}CH_4$ in C_2H_6-contaminated samples, we have observed that the instrument reports heavier values of $\delta^{13}CH_4$ in the presence of C_2H_6. The shift is a result of increased reported $^{13}CH_4$ in samples containing C_2H_6 (see Fig. 8). This is most likely caused by the overlapping of spectral lines within the 6029 wave number region (Rella et al., 2015). We calculate the $\delta^{13}CH_4$ correction by taking the slope of $\Delta\delta^{13}CH_4$ (the difference between the reported $\delta^{13}CH_4$ and the initially reported one of the C_2H_6-free gas) and the corrected C_2H_6 to CH_4 ratio. The ratio is used to permit the calculation of the $\delta^{13}CH_4$ response function per ppm CH_4 as the magnitude of interference is dependent on CH_4 concentration (Rella et al., 2015). The significance of the interference on $\delta^{13}CH_4$ concentrations is illustrated in Fig. 9; as the $C_2H_6 : CH_4$ ratio increases, the change in the reported $\delta^{13}CH_4$ increases linearly. Results obtained from tests carried out throughout the year, for both instruments are noted in Table 3 and plotted in Fig. 9. The correction equation can be expressed as follows:

Table 2. Summary of C_2H_6 calibration factors calculated for both instruments CFIDS 2072 and 2067.

	CFIDS 2072		CFIDS 2067	
C_2H_6 Calibration	Slope	Intercept (ppm)	Slope	Intercept (ppm)
Feb,15	0.49 ± 0.03	0.00 ± 0.01		
Oct,15	0.51 ± 0.01	-0.06 ± 0.04	0.52 ± 0.01	-0.12 ± 0.01

Table 3. The various response functions calculated for the $\delta^{13}CH_4$ correction due to C_2H_6.

	CFIDS 2072		CFIDS 2067	
$\delta^{13}CH_4$ Correction	Slope (‰ CH_4 / C_2H_6)	Intercept (‰)	Slope (‰ CH_4 / C_2H_6)	Intercept (‰)
July,15	$+24 \pm 2$	0.5 ± 0.6	–	–
Nov,15	$+23 \pm 1$	0.2 ± 0.6	$+23 \pm 1$	-2.3 ± 0.7
Nov,15*	$+24 \pm 1$	0.6 ± 0.6	$+24 \pm 2$	-2.5 ± 0.8

* Flask measurement.

$$(\delta^{13}CH_4)_{CORRECTED} = (\delta^{13}CH_4)_{RAW} - E^{*}C_2H_{6\,CORRECTED}/CH_4 + F, \quad (3)$$

where E is the slope of the response function and F is the intercept. E and F are $+23.6 \pm 0.4$ ‰ ppm CH_4 / ppm C_2H_6 and approximately $+0.4 \pm 0.2$ ‰ for instrument CFIDS 2072 and $+23.3 \pm 0.7$ ‰ ppm CH_4 / ppm C_2H_6 and approximately -2.4 ± 0.4 ‰ for instrument CFIDS 2067 respectively. These corrections contain the inherent $\delta^{13}CH_4$ offset of the instrument. When calibrating the $\delta^{13}CH_4$ to a known scale (as described in Sect. 2.5) any instrumental offset will be incorporated within the calibration. Therefore, the correction equations can be simplified to

$$(\delta^{13}CH_4)_{CORRECTED} = (\delta^{13}CH_4)_{RAW} - E^{*}C_2H_{6\,CORRECTED}/CH_4. \quad (4)$$

Also highlighted in Fig. 9 is the typical measurement range for the majority of $ffCH_4$ sources related to dry and wet natural gas relative to calibrated C_2H_6 / CH_4 ratios given on the upper abscissa, whereby dry gas refers to natural gas that occurs in the absence of condensate/liquid hydrocarbons ($C_2H_6 : CH_4 = 1$–6 %) while wet gas typically contains higher concentrations of complex hydrocarbons ($C_2H_6 : CH_4 > 6$ %; Yacovitch et al., 2014). It is clear that within this range the bias on methane isotopic signatures is significant; dry gas will alter the reported $\delta^{13}CH_4$ by 0.8–4 ‰, while wet gas can cause a shift of up to 13 ‰ depending on its $C_2H_6 : CH_4$ ratio.

3.4 $\delta^{13}CH_4$ calibration

Full instrument calibrations as described in Sect. 2.4 were performed once in 2014 and once in 2015. The $\delta^{13}CH_4$ values obtained for the calibration gases by RHUL are measured by IRMS and are therefore not subject to interferences. The calibration gas aliquots were measured with an average standard deviation of 0.03 ‰. To calibrate $\delta^{13}CH_{4\,CORRECTED}$, the $\delta^{13}CH_{4\,CORRECTED}$ was calculated for each calibration gas and used within the linear regression. The calibrations were linear with $R^2 > 0.99$ on both occasions and no change (within our uncertainties) was observed between the two tests. By measuring an ambient air target regularly, we later detected a shift in the $\delta^{13}CH_4$ baseline. Two further calibrations were performed in 2016 to assess this incident which confirmed that the offsets of the linear regressions were significantly shifted, while the slopes agreed well with previous calibrations. Therefore, to account for a baseline drift, it is important to measure a target gas regularly and amend the offset of the calibration equation accordingly.

3.5 Typical instrumental performance and uncertainties

In order to characterize the repeatability of the C_2H_6 measured by the CRDS instrument, we have measured several targets and monitored the changes of the reported C_2H_6 signal over time. The raw signal is a measurement every 3 s, which displays on average a standard deviation of 90 ppb. By aggregating the data to 1 or 30 min intervals, the precision can be improved and a standard deviation of 20 or 8 ppb is reached. Furthermore, the 1 min standard deviation at 52 ppm C_2H_6 is 180 ppb. Thus by assuming a linear relationship the typical performance for 1 min averages is 20 ppb ±0.3 % of reading.

Of course, there are some substantial uncertainties attributed with the C_2H_6 correction and calibration which need to be accounted for when discussing the uncertainty of the calibrated C_2H_6 concentrations. With regards to the C_2H_6

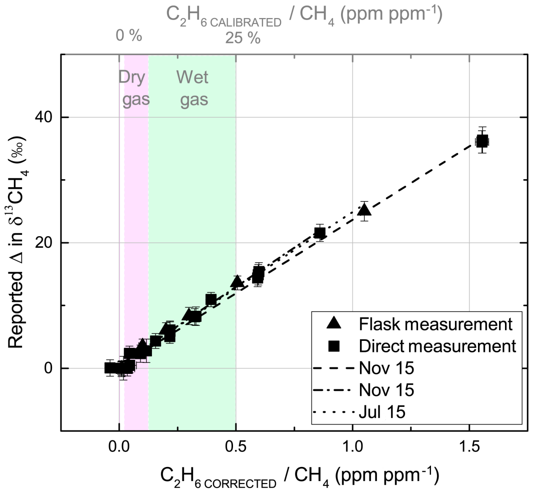

Figure 9. The effect of C_2H_6 on reported $\delta^{13}CH_4$. The slopes of reported $\delta^{13}CH_4$ vs. the $C_2H_{6\,\mathrm{CORRECTED}}$: CH_4 ratio are shown for three tests taken throughout the course of 1 year. Triangular markers imply whole-air sample measurements, while square markers are derived from direct measurements. Error bars indicate the standard deviation. In the presence of C_2H_6 the instrument reports heavier values of $\delta^{13}CH_4$. The typical range of (calibrated) C_2H_6 : CH_4 of dry and wet gas are highlighted in pink and green respectively, corresponding to the top axis.

correction for 1 min averages, if measuring dried ambient air the propagation of uncertainties are negligible with respect to the raw instrumental precision (20 ppb). However, if using 30 min averages the uncertainty augments from 8 to 10 ppb. Elevated CH_4, CO_2 and H_2O signals (> 5 ppm, > 1000 ppm, > 0.2 % respectively) will induce increased C_2H_6 uncertainty regardless of aggregation time. After calibration, the correction factor increases to $2^{1/2}$ times that of the corrected C_2H_6, so at ambient air concentrations calibrated C_2H_6 has an uncertainty of 30 ppb.

The repeatability of $\delta^{13}CH_4$ for 1 min averages on our instrument is a standard deviation of 0.66 ‰. The standard deviation is reduced to 0.29 and 0.09 ‰ by aggregating the raw data for 5 and 30 min respectively. For the correction of $\delta^{13}CH_4$ due to C_2H_6, error propagation of the factors applied in Eq. (4) must be taken into account. Therefore, at ambient concentrations, the uncertainty of a 1 min average will increase to 0.9 ‰.

3.6 Generalizability of corrections and calibrations

The experiments in this study were repeated multiple times and performed on two instruments to better understand how the instrument responses change over time and how they vary between instruments. The C_2H_6 correction and calibration, and $\delta^{13}CH_4$ correction experiments were repeated on CFIDS 2072 over the course of a year to determine any temporal drifts.

The coefficients of the C_2H_6 correction were examined over a 4-month period. Methane, carbon dioxide and water vapour coefficients for dried gas displayed no noticeable variation over this time frame. Both CH_4 and CO_2 coefficients for undried gas also showed good stability throughout this period; however the undried H_2O coefficient is seen to vary significantly (±0.1 ppm C_2H_6 / % H_2O). As discussed previously, the H_2O correction is subject to a hysteresis effect, which makes analysis of its long-term variation difficult. As we did not find a clear temporal pattern of the variations, we therefore suggest that this coefficient is not likely to be time dependent.

The calibration of C_2H_6 was calculated twice within a 9-month period (see Table 2). No variation of the slope of the response function is observed within this time frame. The intercept is prone to drift in time as discussed previously.

The $\delta^{13}CH_4$ correction has been examined three times throughout a 6-month period (see Table 3). The variability of the slope observed over 6 months is 1 ‰ ppm C_2H_6 / ppm CH_4. Given that the error attribution of each experiment is approximately ±1 ‰ ppm C_2H_6 / ppm CH_4, this variability is not statistically significant. The intercepts show good agreement with no variation outside the expected uncertainties.

The comparison of both CRDS instruments showed good agreement for all calculated C_2H_6 correction coefficients, with the exception of the undried H_2O coefficient at > 0.16 % H_2O. For this coefficient we calculate a difference of 0.3 ppmC_2H_6 / % H_2O between that of CFIDS 2072 and CFIDS 2067. The variance may be the consequence of spectrometer differences, a long-term hysteresis effect or differences in their past use (mostly dried samples on CFIDS 2072 and mostly undried samples for CFIDS 2067).

The slopes derived for the C_2H_6 calibration of both instruments correspond well, with no significant difference seen between the two. The intercepts differ by approximately 0.6 ppm, thus suggesting a distinct difference between intra-instrumental C_2H_6 baselines.

The slopes of the $\delta^{13}CH_4$ correction were found to be in good agreement between the two instruments. Where the instruments differ is with regards to their $\delta^{13}CH_4$ baselines, thus causing the observed disparity in intercept (seen in Table 3) of approximately 3 ‰.

To the best of our knowledge, at this time there is only one published study reporting on a correction due to C_2H_6 interference on an isotopic Picarro analyser. Rella et al. (2015) have studied the interference using a Picarro G2132-i, a high-precision CH_4 isotope-only CRDS analyser which uses similar analysis algorithms and spectral regions to that of the Picarro G2201-i. Rella et al. (2015) obtained C_2H_6 correction parameters of $A = 0.658$ ppm C_2H_6 / ppm H_2O, $B = 5.5 \pm 0.1 \times 10^{-3}$ ppm C_2H_6 / ppm CH_4, $C = 1.44 \pm 0.02 \times 10^{-4}$ ppm C_2H_6 / ppm CO_2 in 2015. Factors B and C for CH_4 and CO_2 respectively agree well with the dried air coefficients attained within this study. The H_2O coefficient, as suggested by Rella et al. (2015) differs from both that of CFIDS 2072 and CFIDS 2067 but confirms the variability of this factor between instruments when measuring undried air samples. Lastly, Rella et al. (2015) report a correction factor for $\delta^{13}CH_4$ of 35 ‰ ppm CH_4 / ppm C_2H_6 which indicates a different response to C_2H_6 contamination of the different instrument series.

4 Source identification at a natural gas compressor station

In order to quantify the effect of C_2H_6 contamination in a real world situation, we have applied the corrections and calibrations discussed in this paper to measurements taken at a natural gas site, with the aim of distinguishing emissions between two natural gas pipelines. In the following section we demonstrate the effect of C_2H_6 interference on $\delta^{13}CH_4$ at a fossil fuel site and discuss the alternative approach of using calibrated $C_2H_6 : CH_4$ ratios to distinguish source signatures, a method which has not been previously tested on a Picarro G2201-i.

4.1 Description of field campaign

4.1.1 Site description

Located in an industrial park in northern Europe, the campaign took place at a natural gas compressor station in summer 2014. Such stations serve the distribution of natural gas; their key purpose is to keep an ideal pressure throughout the transmission pipelines to allow continuous transport from the production and processing of natural gas to its use. The visited compressor site comprises two major pipelines with their corresponding compressors. The two pipelines carry gas of different origins to the site, where after pressurization, they are combined for further transmission. The site topography is flat and open with the surrounding area being predominantly farmland and in close proximity to a major road. $FFCH_4$ emissions were expected to emanate from various sources on site such as the compressors, methane slip from turbines and fugitive emissions due to the high pressure of gas (Roscioli et al., 2015). Other possible methane sources in the nearby region were identified as traffic and agriculture, including a livestock holding situated less than 500m south-west of the site.

4.1.2 Continuous measurements of CH_4, $\delta^{13}CH_4$ & C_2H_6

Two instruments were utilized for continuous measurements throughout the 2-week field campaign: a CRDS instrument (CFIDS 2072, characterized in detail in previous sections) and an automatic gas chromatograph with a flame ionization detector (GC-FID; Chromatotec, Saint-Antoine, France) measuring VOCs (light fraction C_2-C_6 hydrocarbons), described in detail in Gros et al. (2011). They were located at a distance of approximately 200–400 m from the pipelines and compressors.

The air measured by the CRDS instrument was dried consistently to < 0.16 % H_2O using a Nafion (Perma Pure LLC, Lakewood, USA). The $\delta^{13}CH_4$ was calibrated using the method described previously in Sect. 2. Every two days, 20 min measurements of two calibration gases were made to calibrate the CH_4 and CO_2 data and to track any drift in the isotopes. A C_2H_6 free working gas was measured every 12 h and used simultaneously as a target gas for the calibration of CH_4 and CO_2, and to track any drift in the C_2H_6 baseline for the calibration of C_2H_6.

The GC-FID was calibrated at the beginning and end of the campaign using a certified standard gas mixture (NPL, National Physics Laboratory, Teddington, UK). The sampling time is a 10 min average every half an hour; 10 min of ambient air is measured after which the following 20 min are used to analyse the input.

4.1.3 Grab sample measurements of CH_4, $\delta^{13}CH_4$ & C_2H_6 in pure natural gas samples

Grab samples of pure natural gas were taken of both pipelines, with the aim of characterizing the two differing gas supplies. The 0.8 L stainless steel flasks were evacuated prior to sampling to a pressure of the order of 10^{-6} mbar, after which they were filled to ambient pressure when sampling. The flasks were measured independently in the laboratory with a manual GC (described in Sect. 2.4) and, after dilution with zero air, by the CRDS instrument.

4.2 Impact of C_2H_6 on $\delta^{13}CH_4$ observations at the field site

To quantify the effect of C_2H_6 interference on $\delta^{13}CH_4$ a total of 16 events were selected from the 2-week field campaign, with criteria defined as a peak exhibiting both increasing CH_4 concentrations and a change in $\delta^{13}CH_4$ signature for a minimum of 1 h. Two such events are plotted in Fig. 10. Event 1 represents the majority of events measured during the field campaign, in which CH_4 and C_2H_6 are well correlated. This particular event has a maximum concentration of 11 ppm CH_4 and 0.6 ppm C_2H_6. On average the selected events have peak concentrations of 5 ppm CH_4 and 0.3 ppm C_2H_6. The methane isotopic signature was char-

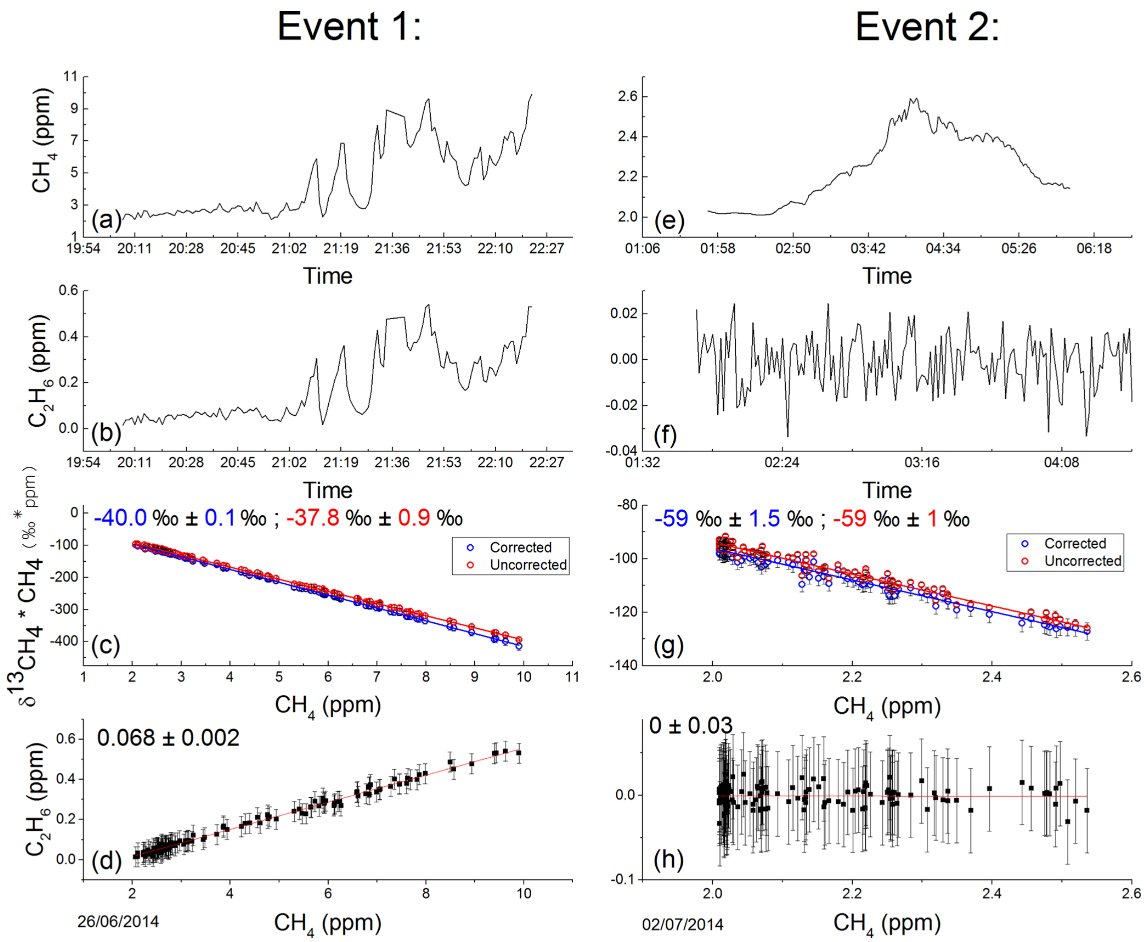

Figure 10. Ethane and methane content of two selected peaks. Methane and ethane 1 min averaged time series is shown in **(a)** and **(b)** for Event 1 and **(e)** and **(f)** for Event 2. Miller–Tans plots of the corresponding peaks are shown in **(c)** and **(g)**, blue for the corrected δ^{13}CH$_4$ due to C_2H_6, and red representing uncorrected δ^{13}CH$_4$. Event 1 includes elevated C_2H_6 emissions and thus displays a difference between the slope before and after C_2H_6 correction, corresponding to a shift in isotopic signature. Event 2, with no C_2H_6 shows no alteration in slope. The slopes of C_2H_6 vs. CH_4 are shown in **(d)** and **(h)**, signifying the $C_2H_6 : CH_4$ ratio of the emission. Errors of both the isotopic and $C_2H_6 : CH_4$ signatures are calculated from the standard error of the slope.

acterized using the Miller–Tans method (Miller and Tans, 2003), in which $\delta^{13}CH_4^*$ CH_4 values are plotted against CH_4 to calculate the isotopic signature of the methane source in situations where the background is not constant. In order to avoid bias stemming from using ordinary least squared (OLS) regression, the York least squares fitting method was implemented, thus taking into account both the X and Y errors (York, 1968). All events excluding one were found to have $\delta^{13}CH_4$ signatures characteristic of natural gas, corresponding on average to −40 ‰. A single event (Event 2 plotted in Fig. 10) was detected with a $\delta^{13}CH_4$ signature of −59 ‰ ± 1.5 ‰. Such a signature suggests a biogenic source and, due to the south-westerly wind direction throughout the event (where the livestock holding is located), suggests the source is likely to originate from livestock, either as ruminant or manure emissions.

If the data are left uncorrected, sources containing C_2H_6 substantially bias the calculated isotopic signature of CH_4 events. This is demonstrated in Fig. 10c where, for Event 1, the slope of points after C_2H_6 correction (in blue) is shifted in comparison to the slope derived from points left uncorrected (in red), signifying a modification of the $\delta^{13}CH_4$ signature. Corrected $\delta^{13}CH_4$ suggests a signature of −40.0 ‰ ± 0.1 ‰, while uncorrected values imply −37.8 ‰ ± 0.08 ‰. When no C_2H_6 is present, i.e. Event 2, there is no disparity between the raw and corrected $\delta^{13}CH_4$ slope, resulting in a $\delta^{13}CH_4$ signature of −59 ‰ ± 1 ‰ for both methods. For the 15 natural-gas-related events, the average shift induced due to uncorrected data is 2 ‰. Consequently the bias in isotopic signatures due to C_2H_6 means that uncorrected data will always overestimate the source when a simple two end-member mixing model is applied.

4.3 Continuous field measurements of ethane

As an independent verification of the CRDS performance we compared two time series of C_2H_6 which were measured simultaneously by the CRDS and GC-FID during the natural gas field campaign by using a co-located air inlet. The CRDS data were averaged to identical time stamps as the GC-FID, i.e. a 10 min average every 30 min. From which we calculated a root mean squared error (RMSE) of 13 ppb. Given the precision of C_2H_6 measured by the CRDS instrument is 10 ppb for 10 min averages, and the uncertainty on the GC-FID is 15 %, we conclude that this is an extremely good agreement.

Furthermore, the flask samples, taken on the 4 July 2014, were measured by the CRDS to have a $C_2H_6 : CH_4$ ratio of 0.074 ± 0.001 ppm C_2H_6 / ppm CH_4 and 0.046 ± 0.003 ppm C_2H_6 / ppm CH_4 for the gas within Pipeline 1 and Pipeline 2 respectively. On the same day gas quality data from the on-site GC recorded a $C_2H_6 : CH_4$ ratio of 0.075 ppm C_2H_6 / ppm CH_4 and 0.048 ppm C_2H_6 / ppm CH_4 respectively. Although the error associated with the later figures is unknown, the strong agreement between the two verifies our correction and calibration strategy of C_2H_6.

4.4 Use of continuous observations of C_2H_6: CH_4 by CRDS

The instruments' capability to now measure interference-corrected and calibrated C_2H_6 opens the door for using another proxy for source apportionment, namely the $C_2H_6 : CH_4$ ratio (Yacovitch et al., 2014, Roscioli et al., 2015, Smith et al., 2015). The $C_2H_6 : CH_4$ ratio that characterizes each source is determined by the slope of the C_2H_6 to CH_4 relationship. This method was applied to the 16 events identified within the natural gas field campaign, again using the York linear regression method, taking into account both X and Y error. Two examples of this method are displayed in the bottom panel of Fig. 10. Event 1, representing a natural gas emission has a measured $C_2H_6 : CH_4$ ratio of 0.068 ± 0.002 ppm C_2H_6 / ppm CH_4, suggesting a wet gas source. Biogenic events, such as Event 2, are absent of C_2H_6 (within our detection limit), thus resulting in a $C_2H_6 : CH_4$ ratio of 0 ± 0.2 ppm C_2H_6 / ppm CH_4. Excluding the biogenic event, on average the 15 natural gas emissions detected have a weighted mean $C_2H_6 : CH_4$ ratio of 0.069 ppm C_2H_6 / ppm CH_4 with an average event uncertainty of 0.006 ppm C_2H_6 / ppm CH_4. This figure agrees well with the median value for conventional gas ratios measured by Roscioli et al. (2015).

If the C_2H_6 data are left uncorrected and uncalibrated the $C_2H_6 : CH_4$ ratio calculated is significantly shifted by approximately +0.06. The average raw $C_2H_6 : CH_4$ ratio for the 15 natural gas events is 0.132 ± 0.007 ppm C_2H_6 / ppm CH_4, while the biogenic events $C_2H_6 : CH_4$ ratio calculated is negative and thus impossible.

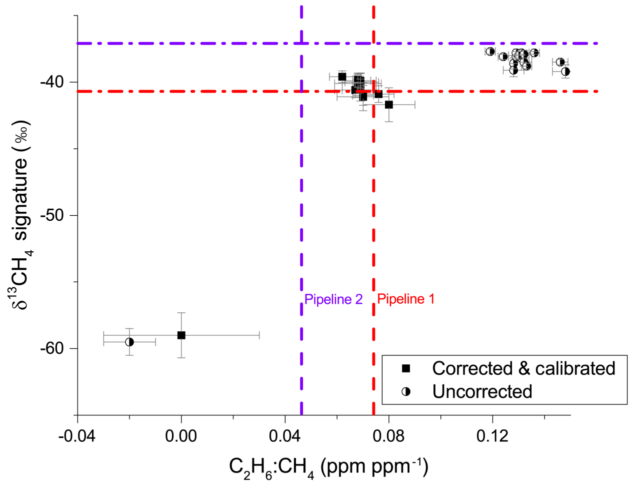

Figure 11. Distribution of 16 events according to their $C_2H_6 : CH_4$ ratios and isotopic signature. The red and purple dashed lines signify the characterizations of Pipeline 1 and 2 respectively as measured by the CRDS instrument from flask samples taken on the 4 July 14. For corrected and calibrated data (square markers), both the isotopic signature and $C_2H_6 : CH_4$ ratios identify the biogenic source (bottom-left point) and suggest the natural gas emissions emanate from Pipeline 1. Circular markers represent the uncorrected data which does not agree with the flask sample measurements of pipelines 1 or 2. The error bars indicate the standard error of the slope calculated from Miller–Tans and C_2H_6 vs. CH_4 plots for $\delta^{13}CH_4$ signature and $C_2H_6 : CH_4$ ratio respectively.

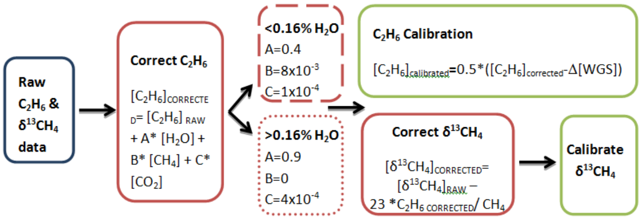

Figure 12. Flow chart illustrating the steps and the corresponding equations to calibrate C_2H_6 and $\delta^{13}CH_4$ as determined from this study. The coefficients are the mean of both CRDS instruments tested. We suggest removing H_2O from gas samples prior to analysis.

4.5 Combined method for CH_4 source apportionment

To distinguish which pipeline the emissions originate from, we compare both the $\delta^{13}CH_4$ signature and the $C_2H_6 : CH_4$ ratio source apportionment methods. The two pipelines were characterized from the whole-air samples taken on 4 July 2014; although the gas within the pipelines is subject to change as incoming gas varies, we assume here that this did not occur throughout the short duration of the campaign (24 June to 4 July 2014). The data collected from the aforementioned 16 events are compiled within Fig. 11, which illustrates the distribution of $\delta^{13}CH_4$ signature vs. $C_2H_6 : CH_4$

ratios. The results from the flask measurements, i.e. characteristics of Pipeline 1 and 2, are plotted as dashed purple and red lines. Both methods clearly identify the biogenic source, seen as an outlier in the bottom left corner of the plot. Furthermore, both methods are able to distinguish between the two pipelines. The isotopic signatures of the natural gas events (on average 40.2 ‰ ± 0.5 ‰) are clustered near the isotopic signature of Pipeline 1, which has a $\delta^{13}CH_4$ signature of 40.7 ‰ ± 0.2 ‰, thus suggesting the majority of the measured methane is an emission from this pipeline. When considering the $C_2H_6:CH_4$ ratio a similar conclusion may be drawn as the mean $C_2H_6:CH_4$ ratio is 0.069 ± 0.002 ppm C_2H_6 / ppm CH_4, much like that of Pipeline 1 at 0.074 ± 0.003. A future study will address the shift in measured events to the left of Pipeline 1 in Fig. 11 by using additional VOC data from the GC-FID to aid source identification. The uncorrected 16 events are also plotted in Fig. 11 as circular markers. These are found in the top right-hand corner of Fig. 11 and do not correspond well with either of the pipelines, thus reconfirming the importance of the corrections.

5 Concluding remarks

This study focuses on measurements of C_2H_6 contaminated methane sources by a CRDS (Picarro G2201-i), with emphasis on correcting $\delta^{13}CH_4$ and (although not intended for use by standard users) C_2H_6 for cross-interferences before calibration. Our extensive laboratory tests suggest that CRDS instruments of this model are all subject to similar interferences (as expected as they scan the same spectral lines) and that they can have a significant impact on reported concentrations and isotopic signatures if not accounted for properly when measuring industrial natural gas sources. For now, we suggest using constant, instrument-specific correction factors if possible or the ones found in this study (summarized in Fig. 12). As our study period only encompasses 1 year it is clear that the stability of the correction over the full life-time needs to be monitored further. To fully exploit the reported C_2H_6 data, we suggest drying gas samples to < 0.16 % H_2O, calibrating the instrument and taking frequent measurements of a working gas (or set of working gases) to monitor and correct for the instrumental baseline drift.

The results of our field campaign demonstrate the extent of the interferences of C_2H_6 on $\delta^{13}CH_4$ for a real world application and also support the validity of our C_2H_6 correction and calibration through the comparison with an independently calibrated GC-FID. In our case, when measuring wet gas emissions we detected an average shift in isotopic signature of 2.5 ‰ due to C_2H_6 interference; however the extent of this bias will vary according to the contribution of C_2H_6, therefore affecting each $ffCH_4$ source to a different degree which can cause problems for source determination. The results reported here are important for all future work of CRDS in fossil fuel regions (where sources consist of a $C_2H_6:CH_4$ ratio between 0 and 1 ppm C_2H_6 / ppm CH_4) to create awareness of such interferences and correct for them accordingly. Our CRDS instrument is sufficient for measurements of strongly variable C_2H_6 sources, where if using calibrated 1 min C_2H_6 data, concentration variations above 150 ppb are required to achieve a signal-to-noise ratio of 5. Thus for industrial natural gas sites it offers a new opportunity to use continuous $C_2H_6:CH_4$ observations as a means of source determination that is independent from $\delta^{13}CH_4$ methods. The recently released G2210-i analyser is dedicated to $C_2H_6:CH_4$ ratio measurements and as such achieves a higher precision, making it suitable for a wider variety of ethane sources.

Finally, we successfully combined both the $\delta^{13}CH_4$ and $C_2H_6:CH_4$ ratio source apportionment methods. At the natural gas compressor site both methods clearly distinguish biogenic sources from that of natural-gas-based sources. Combining those two independent methods yields a better fingerprint of the source and spurious C_2H_6 or $\delta^{13}CH_4$ can be more easily identified. Lastly, by characterizing both the $\delta^{13}CH_4$ and $C_2H_6:CH_4$ ratio of our source, we gain insight into the formation and source region of the gas (Schoell, 1983).

Code and data availability. Code and data are available on request.

The Supplement related to this article is available online at https://doi.org/10.5194/amt-10-2077-2017-supplement.

Competing interests. The authors declare that they have no conflict of interest.

Acknowledgements. The authors would like to thank the NPL team for organizing the field campaign, in particular the support from Rod Robinson, Fabrizio Innocenti and Andrew Finlayson. We thank our LSCE colleagues: Camille Yver Kwok and Sebastien Ars for assistance during the field campaign, as well as Bernard Bonsang and Dominique Basinee for their technical help and contributions on the GC instruments both on and off the field. We also thank Rebecca Fisher (RHUL) and Dave Lowry for their contributions, especially for measurements of $\delta^{13}CH_4$ for our calibration cylinders under the InGOS' TransNational Access programme (TNA-id-666; http://www.ingos-infrastructure.eu/project-info/workpackages/tna-transnational-access/). This work was supported by the Climate KIC through the FuME project (http://www.climate-kic.org/projects/fume/) and the funding of the PhD studies of Sabina Assan through the education of climate KIC.

Edited by: M. Hamilton
Reviewed by: three anonymous referees

References

Allen, D. T.: Methane emissions from natural gas production and use: reconciling bottom-up and top-down measurements, Current Opinion in Chemical Engineering, 5, 78–83, 2014.

Bonsang, B. and Kanakidou, M.: Nonmethane hydrocarbon measurements during the FIELDVOC 1994 experiment, Chemosphere, Global Change Science, 3, 259–273, 2001.

Fisher, R., Lowry, D., Wilkin, O., Sriskantharajah, S.. and Nisbet, G.: High- precision, automated stable isotope analysis of atmospheric methane and carbon dioxide using continuous-flow isotope-ratio mass spectrometery, Rapid Commun. Mass Spectrom., 20, 200–208, 2006.

Gilman, J. B., Lerner, B. M., Kuster, W. C., and De Gouw, J. A.: Source signature of volatile organic compounds from oil and natural gas operations in northeastern Colorado, Environ. Sci. Technol., 47, 1297–1305, 2013.

Gros, V. , Gaimoz, C., Herrmann, F., Custer, T., Williams, J., Bonsang, B., Sauvage, S., Locoge, N., d'Argouges, O., Sarda-Estève, R., and Sciare, J.: Volatile Organic Compounds Sources in Paris in spring 2007. Part I: qualitative analysis, Environ. Chem., 8, 74–90, 2011.

Hiller, R. V., Bretscher, D., DelSontro, T., Diem, T., Eugster, W., Henneberger, R., Hobi, S., Hodson, E., Imer, D., Kreuzer, M., Künzle, T., Merbold, L., Niklaus, P. A., Rihm, B., Schellenberger, A., Schroth, M. H., Schubert, C. J., Siegrist, H., Stieger, J., Buchmann, N., and Brunner, D.: Anthropogenic and natural methane fluxes in Switzerland synthesized within a spatially explicit inventory, Biogeosciences, 11, 1941–1959, https://doi.org/10.5194/bg-11-1941-2014, 2014.

Höglund-Isaksson, L.: Global anthropogenic methane emissions 2005–2030: technical mitigation potentials and costs, Atmos. Chem. Phys., 12, 9079–9096, https://doi.org/10.5194/acp-12-9079-2012, 2012.

Jackson, R. B., Down, A., Phillips, N. G., Ackley, R. C., Cook, C. W., Plata, D. L., and Zhao, K.: Natural gas pipeline leaks across Washington, DC, Environ. Sci. Technol., 48, 2051–2058, 2014.

Kirschke, S., Bousquet, P., Ciais, P., Saunois, M., Canadell, J. G., Dlugokencky, E., Bergamaschi, P., Bergmann, D., Blake, D., Bruhwiler, L., Cameron-Smith, P., Castaldi, S., Chevallier, F., Feng, L., Fraser, A., Heimann, M., Hodson, E., Houweling, S., Josse, B., Fraser, P. J., Krummel, P. B., Lamarque, J., Langenfelds, R. L., Le Quéré, C., Naik, V., O'Doherty, S., Palmer, P. I., Pison, I., Plummer, D., Poulter, B., Prinn, R. J., Rigby, M., Ringeval, B., Santini, M., Schmidt, M., Shindell, D. T., Simpson, I. J. Spahni, R., Steele, l. P., Strode, S. A., Sudo, K., Szopa, S., van der Werf, G. R., Voulgarakis, A., van Weele, M., Weiss, R. F., Williams, J. E., and Zeng, G.: Three decades of global methane sources and sinks, Nat. Geosci., 6, 813-823, 2013.

Lamb, B. K., McManus, J. B., Shorter, J. H., Kolb, C. E., Mosher, B., Harriss, R. C., Allwine, E., Blaha, D., Howard,T ., Guenther, A., Lott, R. A., Siverson, R., Westburg, H., and Zimmerman, P.: Development of atmospheric tracer methods to measure methane emissions from natural gas facilities and urban areas, Environ. Sci. Technol., 29, 1468–1479, 1995.

Laurent, O. et al.: Icos ATC Metrology Lab: Metrological performance assessment of GHG analyzers, Atmospheric Measurement Techniques 8.10 4075–4082, Poster session presented at: 18th WMO/IAWA Meeting on Carbon Dioxide, Other Greenhouse Gases, and Related Measurement Techniques (GGMT), 13–17 September, California, CA, 2015.

Lowry, D., Holmes, C. W., Rata, N. D., O'Brien, P., and Nisbet, E. G.: London methane emissions: Use of diurnal changes in concentration and δ13C to identify urban sources and verify inventories, J. Geophys. Res.-Atmos., 106, 7427–7448, 2001.

Malowany, K., Stix, J., Van Pelt, A., and Lucic, G.: H_2S interference on CO_2 isotopic measurements using a Picarro G1101-i cavity ring-down spectrometer, Atmos. Meas. Tech., 8, 4075–4082, https://doi.org/10.5194/amt-8-4075-2015, 2015.

Miller, J. B. and Tans, P. P.: Calculating isotopic fractionation from atmospheric measurements at various scales, Tellus B, 55.2, 207–214, 2003.

Nara, H., Tanimoto, H., Tohjima, Y., Mukai, H., Nojiri, Y., Katsumata, K., and Rella, C. W.: Effect of air composition (N_2, O_2, Ar, and H_2O) on CO_2 and CH_4 measurement by wavelength-scanned cavity ring–down spectroscopy: calibration and measurement strategy, Atmos. Meas. Tech., 5, 2689–2701, https://doi.org/10.5194/amt-5-2689-2012, 2012.

Phillips, N. G., Ackley, R., Crosson, E. R., Down, A., Hutyra, L. R., Brondfield, M., Karr, J. D., Zhao, K., and Jackson, R. B.: Mapping urban pipeline leaks: Methane leaks across Boston, Environ. Pollut., 173, 1–4, 2013.

Rella, C. W., Hoffnagle, J., He, Y., and Tajima, S.: Local- and regional-scale measurements of CH_4, $\delta^{13}CH_4$, and C_2H_6 in the Uintah Basin using a mobile stable isotope analyzer, Atmos. Meas. Tech., 8, 4539–4559, https://doi.org/10.5194/amt-8-4539-2015, 2015.

Roscioli, J. R., Yacovitch, T. I., Floerchinger, C., Mitchell, A. L., Tkacik, D. S., Subramanian, R., Martinez, D. M., Vaughn, T. L., Williams, L., Zimmerle, D., Robinson, A. L., Herndon, S. C., and Marchese, A. J.: Measurements of methane emissions from natural gas gathering facilities and processing plants: measurement methods, Atmos. Meas. Tech., 8, 2017–2035, https://doi.org/10.5194/amt-8-2017-2015, 2015.

Schoell, M.: Genetic characterization of natural gases, AAPG bulletin, 67, 2225–2238, 1983.

Smith, M. L., Kort, E. A., Karion, A., Sweeney, C., Herndon, S. C., and Yacovitch, T. I.: Airborne ethane observations in the Barnett shale: Quantification of ethane flux and attribution of methane emissions, Environ. Sci. Technol., 49, 8158–8166, 2015.

Stevens, C. M. and Engelkemeir, A.: Stable carbon isotopic composition of methane from some natural and anthropogenic sources, J. Geophys. Res.-Atmos., 93, 725–733, 1988.

Subramanian, R., Williams, L. L., Vaughn, T. L., Zimmerle, D., Roscioli, J. R., Herndon, S. C., Yacovitch, T. L., Floerchinger, C., Tkacik, D. S., Mitchell, A. L., Sullivan, M. R., Dallmann, T. R., and Robinson, A. L.: Methane emissions from natural gas compressor stations in the transmission and storage sector: Measurements and comparisons with the EPA greenhouse gas reporting program protocol, Environ. Sci. Technol., 49, 3252–3261, 2015.

US Environmental Protection Agency: Inventory of U.S Greenhouse Gas Emissions and Sinks: 1990–2014, EPA 430-R-16-002, Annex 7, available at: https://www3.epa.gov/climatechange/Downloads/ghgemissions/US-GHG-Inventory-2016-Annex-7-Uncertainty.pdf (last access: 2 May 2017), 2016.

Vogel, F. R., Huang, L., Ernst, D., Giroux, L., Racki, S., and Worthy, D. E. J.: Evaluation of a cavity ring-down spectrometer for in situ observations of $^{13}CO_2$, Atmos. Meas. Tech., 6, 301–308, https://doi.org/10.5194/amt-6-301-2013, 2013.

Yacovitch, T. I., Herndon, S. C., Roscioli, J. R., Floerchinger, C., McGovern, R. M., Agnese, M., Pétron, G., Kofler, J., Sweeney, C., Karion, A., Conley, S. A., Kort, E. A., Nähle,L., Fischer, M., Hildebrandt,L., Koeth,J., McManus, J. B., Nelson, D. D., Zahniser, M. S., and Kolb, C. E.: Demonstration of an ethane spectrometer for methane source identification, Environ. Sci. Technol., 48, 8028–8034, 2014.

Yacovitch, T. I., Herndon, S. C., Pétron, G., Kofler, J., Lyon, D., Zahniser, M. S., and Kolb, C. E.: Mobile laboratory observations of methane emissions in the Barnett Shale region, Environ. Sci. Technol., 49, 7889–7895, 2015.

York, D.: Least squares fitting of a straight line with correlated errors, Earth Planet. Sc. Lett., 5, 320–324, 1968.

Yvon-Lewis, S. A., Hu, L., and Kessler, J.: Methane flux to the atmosphere from the Deepwater Horizon oil disaster, Geophys. Res. Lett., 38, L01602, https://doi.org/10.1029/2010GL045928, 2011.